Int. J. Electrochem. Sci., 15 **(2020)** 4798 – 4810, doi: 10.20964/2020.05.91

International Journal of
ELECTROCHEMICAL
SCIENCE
www.electrochemsci.org

One-pot Synthesis of Pd-$PdH_{0.706}$@PdO-NiO_xH_y/C Core-shell Anode Catalyst with High Activity for Methanol Oxidation

Dengke Wen, Yuming Wu, Xuli Ma, Xiuping Yue, Meisheng Liang, Lizhen Gao, Shaohui Yan[*]

College of Environmental Science and Engineering, Taiyuan University of Technology, Taiyuan, 030024, China
[*]E-mail: yanshaohui@tyut.edu.cn

Received: 3 January 2020 / *Accepted:* 4 March 2020 / *Published:* 10 April 2020

To improve the performance of direct methanol fuel cells (DMFCs), activated carbon-decorated palladium and nickel nanocatalysts (Pd-$PdH_{0.706}$@PdO-NiO_xH_y/C) with high performance were synthesized by a one-pot solvothermal method. A transmission electron microscopy (TEM) analysis of the Pd-$PdH_{0.706}$@PdO-NiO_xH_y/C catalyst reveals that the average diameter of their metal nanoparticles is approximately 10 nm. An X-ray powder diffraction (XRD) analysis suggests that Pd hydride ($PdH_{0.706}$) is synthesized successfully on Pd-$PdH_{0.706}$@PdO-NiO_xH_y/C. In addition, an X-ray photoelectron spectroscopy (XPS) analysis shows that the geometric structure of the particles is mostly spherical and shows a core-shell structure with the shell consisting of PdO-NiO and the core consisting of Pd-$PdH_{0.706}$. Moreover, $Ni(OH)_2$ and $PdH_{0.706}$ can increase Pd activity, and $Ni(OH)_2$ is catalytically active towards the methanol oxidation reaction. Therefore, the Pd-$PdH_{0.706}$@PdO-NiO_xH_y/C catalysts have high catalytic activity for methanol oxidation and ethanol oxidation. A cyclic voltammetry (CV) analysis indicates that the highest oxidation peak values of the Pd-$PdH_{0.706}$@PdO-NiO_xH_y/C catalysts is 592.1 and 1504.0 mA mg^{-1} Pd for methanol oxidation and ethanol oxidation, respectively. According to results of the chronoamperometry (CA) and electrochemical impedance spectroscopy (EIS) tests, the Pd-$PdH_{0.706}$@PdO-NiO_xH_y/C catalysts exhibit excellent activity and durability, as well as an outstanding charge transfer rate.

Keywords: Pd nanoparticles, $PdH_{0.706}$ nanoparticles, $Ni(OH)_2$, Ethanol electrooxidation, Methanol electrooxidation

1. INTRODUCTION

DMFCs have attracted increasing worldwide attention due to their highly efficient and pollution-free operation, excellent properties, ease of use and other features [1-3]. In addition, an electrocatalyst is an essential part of methanol fuel cells [4,5]. To date, Pt catalysts, which show good activity and stability, are the most developed catalysts for the electrochemical oxidation of alcohols [6]. However, as one of the materials in methanol oxidation, the active reaction sites of the Pt catalysts can be occupied by CO, thereby impeding reaction kinetics [7,8]. Additionally, the high cost of Pt needs to be considered [9,10].

Due to the potential tunability of Pd to provide excellent performance and catalytic activity, studies of nanocrystals, especially Pd nanoparticles or their alloy clusters, have been extensively studied in current research [11,12]. Pd has a higher catalytic activity for oxidative deoxygenation of small molecular alcohols than Pt in alkaline media [13,14]. In addition, the size and morphology of Pd nanostructures are effectively regulated by the highly scattered Ni particles on a support with a large surface area [15,16].Thus, the preparation of Pd-Ni alloy catalysts is an effective way to significantly improve the overall catalytic activities of Pd [17,18]. In addition, strategies for forming palladium hydrides appear to be very promising. Recently, $PdH_{0.33}$ nanodendrites have been demonstrated to possess significantly improved ORR activity [19]. The hydride degree of the Pd nanostructures (PdH_x) plays an important role in the enhancement of their oxygen reduction reaction (ORR) activity [20].

The common standards for a high-performance catalyst are (1) a nanoscale-size distribution [21]; (2) a uniform composition throughout the metal nanoparticles [22]; and (3) high dispersion on the carbon support [23]. To attain these standards, the electrocatalyst preparation methods are important [24]. The main disadvantage of an impregnation method is that it is difficult to control the nanoparticle size and distribution [25]. A microemulsion method consumes a large amount of surfactant, requires a large number of separation and washing steps, and may not be suitable for large-scale production [25]. Therefore, it is necessary to introduce a simple method for preparing a Pd-Ni catalyst by a solvothermal method. Moreover, the structure-directing agent of a solvothermal method is also important for the preparation of catalysts. Tert-butanol (TBA) demonstrates unique viscosity and hydrophobicity due to its unique spatial structure and is usually used as a structure-directing agent for preparing catalysts [26].

Here, a $Pd\text{-}PdH_{0.706}@PdO\text{-}NiO_xH_y/C$ nanocatalyst is synthesized with TBA and KOH solution, and it is found that $Pd\text{-}PdH_{0.706}$ is successively synthesized on activated carbon, with the aim to improve the efficiency of the DMFC anode catalyst. In this study on the $Pd\text{-}PdH_{0.706}@PdO\text{-}NiO_xH_y/C$ catalysts, the effect of the amount of KOH solution, average particle size, and nanoparticle distribution on the catalytic activity are fully discussed.

2. EXPERIMENTAL

2.1 Synthesis of the $Pd\text{-}PdH_{0.706}@PdO\text{-}NiO_xH_y/C$ catalysts

The $Pd\text{-}PdH_{0.706}@PdO\text{-}NiO_xH_y/C$ catalysts are prepared by a solvothermal method. In a typical experiment, 0.048 g activated carbon was mixed with 2 ml of 0.0564 M $PdCl_2$ solution, 1 ml of 0.1128 M $NiCl_2$ and 35 ml of TBA in a 50-ml beaker (the molar ratio of Pd to Ni is kept at approximately 1:1). The beaker was stirred with ultrasonication for 30 min. Then, an appropriate amount of 1 M KOH solution was added to adjust the pH value of the suspension. Starting from 8 ml, the suspension was made alkaline with a KOH solution. Then, it was poured into a stainless-steel reaction kettle lined with Teflon, which was placed in an oven and heated to 180 °C for 6 hours. The reaction mixture was cooled to room temperature, and then carefully filtered and rinsed thoroughly with distilled water and anhydrous ethanol. Next, it was desiccated at 80°C for 6 hours in a vacuum drying oven, ground with an agate mortar, and kept in a plastic tube. Thus, a Pd-$PdH_{0.706}$@PdO-NiO_xH_y/C catalyst was obtained. The prepared catalyst was denoted as Pd-$PdH_{0.706}$@PdO-NiO_xH_y/C-a. The value of "a" was the amount of 1 M KOH solution added to the reaction system. Thus, the catalysts were labelled Pd-$PdH_{0.706}$@PdO-NiO_xH_y/C-8, Pd-$PdH_{0.706}$@PdO-NiO_xH_y/C-9, Pd-$PdH_{0.706}$@PdO-NiO_xH_y/C-10, and Pd-$PdH_{0.706}$@PdO-NiO_xH_y/C-11.

2.2 Characterization of the Pd-$PdH_{0.706}$@PdO-NiO_xH_y/C catalysts

The metal content of the nanocatalyst was measured by applying atomic absorption spectrometry 6000 (AAS). The morphologies of the Pd-$PdH_{0.706}$@PdO-NiO_xH_y/C catalyst supported on activated carbons were characterized using a JEM 1200EX field emission gun TEM device. XRD was performed using a Rigaku D/Max Ultima II diffractometer with Cu Ka radiation (k = 0.15418 nm). XPS was performed with a Thermo Scientific Esca-lab 250Xi instrument.

2.3 Electrochemical measurements

Electrochemical tests were performed using a three-electrode system. The working electrode was fabricated according to the method described in the literature [26-28]. A graphite electrode (4 cm^2) and an Ag/AgCl electrode were used as the counter and reference electrodes, respectively. The testing electrolytes were deoxygenated solutions of 0.05 M H_2SO_4, 0.1 M KOH + 1 M CH_3OH and 0.1 M KOH + 1 M CH_3CH_2OH. A CHI760E electrochemical workstation (Shanghai, China) was used to record the electrochemical data. All experiments were conducted at 25°C.

3. RESULTS AND DISCUSSION

3.1 Characterization of the Pd-$PdH_{0.706}$@PdO-NiO_xH_y/C catalysts

As shown in Table 1, the AAS analysis reveals that the actual Pd loadings of the Pd-$PdH_{0.706}$@PdO-NiO_xH_y/C catalysts are 15.5, 16.0, 16.5 and 16.1 wt%. The actual Ni loadings of the catalysts are 5.6, 5.9, 6.4 and 5.0 wt%. Both the Pd loading and Ni loading are lower than the theoretical total metal loading due to the incomplete reduction of Pd^{2+} [27]. It can be seen that the amount of KOH solution affects the reduction of the metal. The actual total metal loading first increases and then decreases with increasing pH during preparation. Therefore, the KOH solution value can accelerate the rate of the Pd reduction reaction, promote the rapid nucleation of Pd particles, and produce uniform Pd particles required for high activity [28]. The maximum actual total metal loading is in the Pd-$PdH_{0.706}$@PdO-NiO_xH_y/C-10 catalyst.

Table 1. Metal loading of the Pd-$PdH_{0.706}$@PdO-NiO_xH_y/C catalysts measured by AAS

Catalyst	Pd loading (wt%)	Ni loading (wt%)	Actual total metal loading (wt%)	Theoretical total metal loading (wt%)
Pd-PdH$_{0.706}$@PdO-NiO$_x$H$_y$/C-8	15.5	5.6	21.1	27.6
Pd-PdH$_{0.706}$@PdO-NiO$_x$H$_y$/C-9	16	5.9	21.9	27.6
Pd-PdH$_{0.706}$@PdO-NiO$_x$H$_y$/C-10	16.5	6.4	22.9	27.6
Pd-PdH$_{0.706}$@PdO-NiO$_x$H$_y$/C-11	16.1	5	21.1	27.6

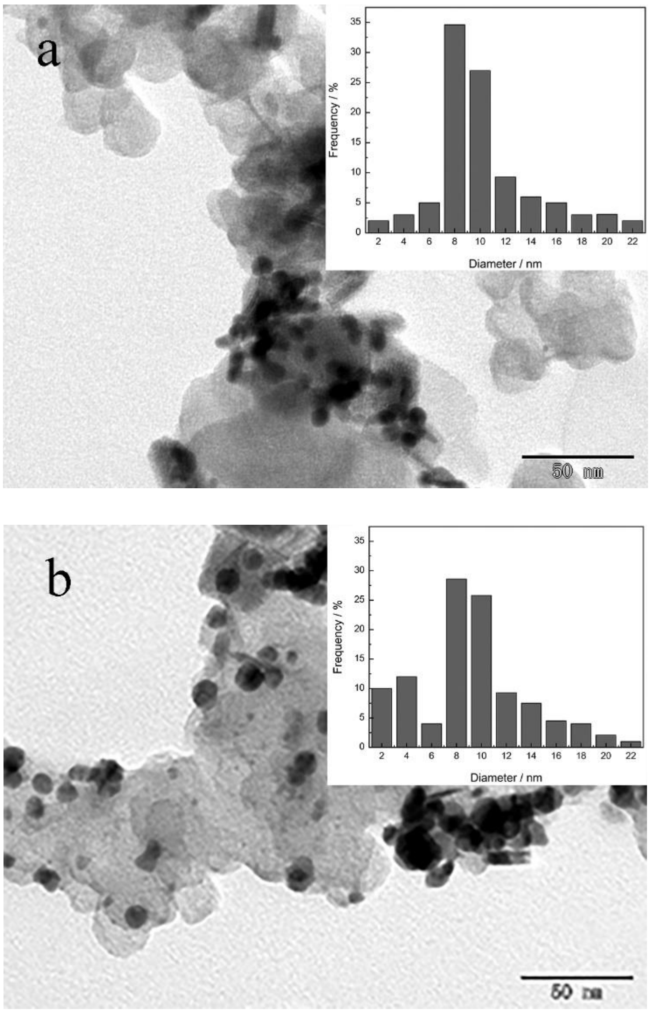

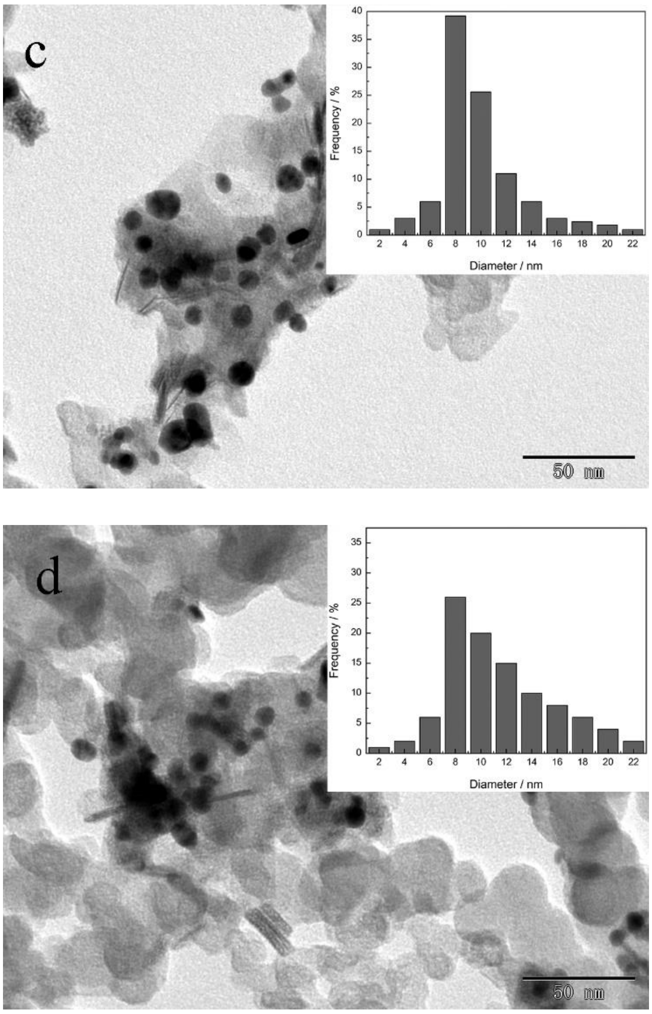

Figure 1. TEM images of the (a) Pd-PdH$_{0.706}$@PdO-NiO$_x$H$_y$/C-8, (b) Pd-PdH$_{0.706}$@PdO-NiO$_x$H$_y$/C-9, (c) Pd-PdH$_{0.706}$@PdO-NiO$_x$H$_y$/C-10 and (d) Pd-PdH$_{0.706}$@PdO-NiO$_x$H$_y$/C-11 catalysts

TEM was used to study the morphology of the Pd-PdH$_{0.706}$@PdO-NiO$_x$H$_y$/C catalysts. Fig. 1 shows that the Pd-based metal nanoparticles successfully combine with activated carbon. The average diameters of the nanoparticles in the Pd-PdH$_{0.706}$@PdO-NiO$_x$H$_y$/C-8, Pd-PdH$_{0.706}$@PdO-NiO$_x$H$_y$/C-9, Pd-PdH$_{0.706}$@PdO-NiO$_x$H$_y$/C-10 and Pd-PdH$_{0.706}$@PdO-NiO$_x$H$_y$/C-11 catalysts are approximately 10.28, 10.03, 9.85 and 11.34 nm, respectively. It can be seen that the average diameter first decreases and then increases with the increase in the amount of KOH solution. The Pd-PdH$_{0.706}$@PdO-NiO$_x$H$_y$/C-10 catalyst has the smallest average diameter. This is because the reaction system is related to the amount of the KOH solution, and the appropriate amount of the KOH solution can increase the loading of the Pd or Pd-Ni metal [29]. In terms of dispersion, some agglomerations of the Pd-based nanoparticles occur on the activated carbon. However, the Pd-PdH$_{0.706}$@PdO-NiO$_x$H$_y$/C-10 catalyst has the least agglomeration on the activated carbon. It can be clearly seen that the distribution of the Pd-PdH$_{0.706}$@PdO-NiO$_x$H$_y$/C-10 catalyst is more uniformly dispersed than other catalysts. Therefore, the dispersion of the metal nanoparticles increases with the amount of KOH solution. This is because the amount of KOH solution affects the reduction rate of the Pd and Pd-Ni nanoparticles, which has a profound influence on the size and dispersibility of the nanoparticles [30].

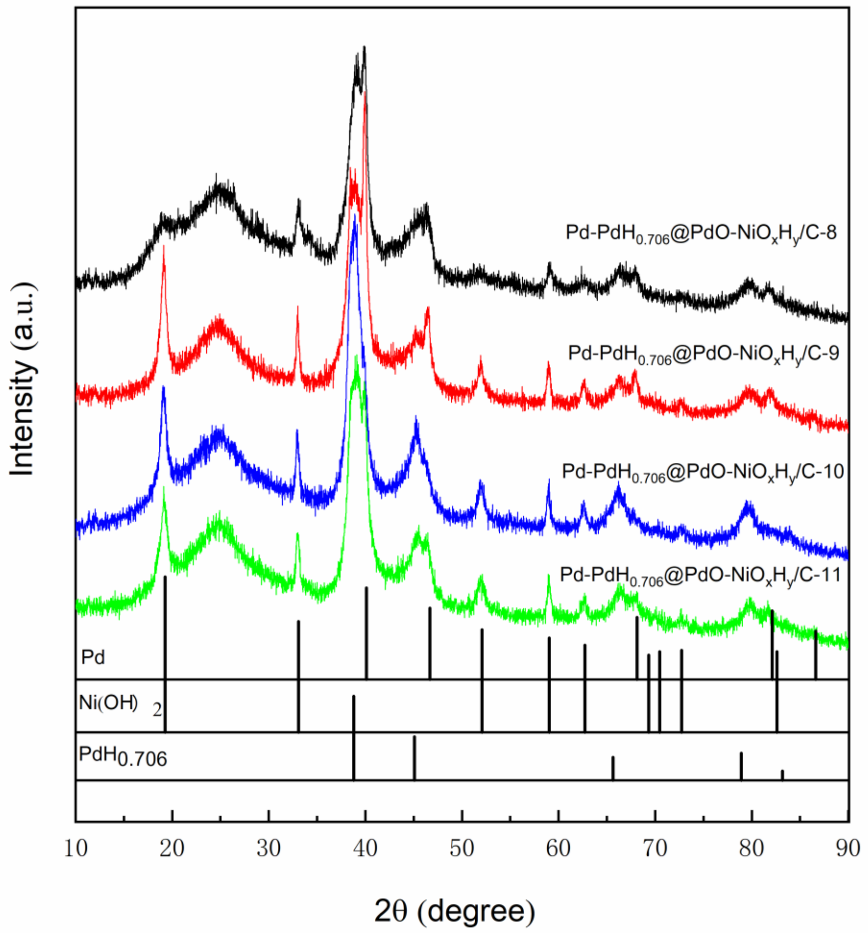

Figure 2. XRD spectra of the Pd-$PdH_{0.706}$@PdO-NiO_xH_y/C-8, Pd-$PdH_{0.706}$@PdO-NiO_xH_y/C-9, Pd-$PdH_{0.706}$@PdO-NiO_xH_y/C-10 and Pd-$PdH_{0.706}$@PdO-NiO_xH_y/C-11 catalysts.

The XRD patterns of the Pd-$PdH_{0.706}$@PdO-NiO_xH_y/C-8, Pd-$PdH_{0.706}$@PdO-NiO_xH_y/C-9, Pd-$PdH_{0.706}$@PdO-NiO_xH_y/C-10 and Pd-$PdH_{0.706}$@PdO-NiO_xH_y/C-11 catalysts are shown in Fig. 2. The standard XRD cards of Pd, $PdH_{0.706}$ and $Ni(OH)_2$ are included for comparison. All catalysts display a large peak at approximately 25°, which corresponds to the (002) plane of the activated carbon support (JCPDS No.98-3439). Furthermore, all catalysts display four peaks at approximately 40.1°, 46.7°, 68.1°, and 82.1°. These peaks are attributed to the Pd (111), (200), (220), and (311) planes, respectively (JCPDS No. 72-0710). The XRD patterns of all the Pd-$PdH_{0.706}$@PdO-NiO_xH_y/C catalysts reflect an fcc crystalline structure. The formation of $PdH_{0.706}$ is also confirmed by an XRD analysis. Relative to the Pd peaks, the diffraction peaks of $PdH_{0.706}$ all shift to low 2θ angles, indicating that the crystal lattice constant has increased [20]. Comparing with the Joint Committee on Powder Diffraction Standards (JCPDS No. 87-637) file, the PdH is between Pd and $PdH_{0.706}$; therefore, the sample can be assigned as Pd-$PdH_{0.706}$. Pd nanocrystals may form first and then transform in situ to $PdH_{0.706}$ [31]. TBA has a boiling point of 82.3 °C, so TBA may generate methacrylaldehyde at high temperature and pressure in situ. It has been reported that aldehydes produce hydrogen gas on metal catalysts [29]. Therefore, the catalytic decomposition of TBA on the surface of the initially formed Pd nanocrystals provides hydrogen gas, which is then absorbed into the Pd nanocrystals to form $PdH_{0.706}$ at a later growth stage. With the exception of the diffraction peaks of the carbon and Pd nanoparticles, it is found that all the catalysts have five additional peaks located at approximately 19.3°, 33.1°, 52.1°, 59.1° and 62.7° due to $Ni(OH)_2$ (JCPDS No.74-2075) [32]. This indicates that Ni mostly exists in the form of $Ni(OH)_2$ using this preparation method [33].

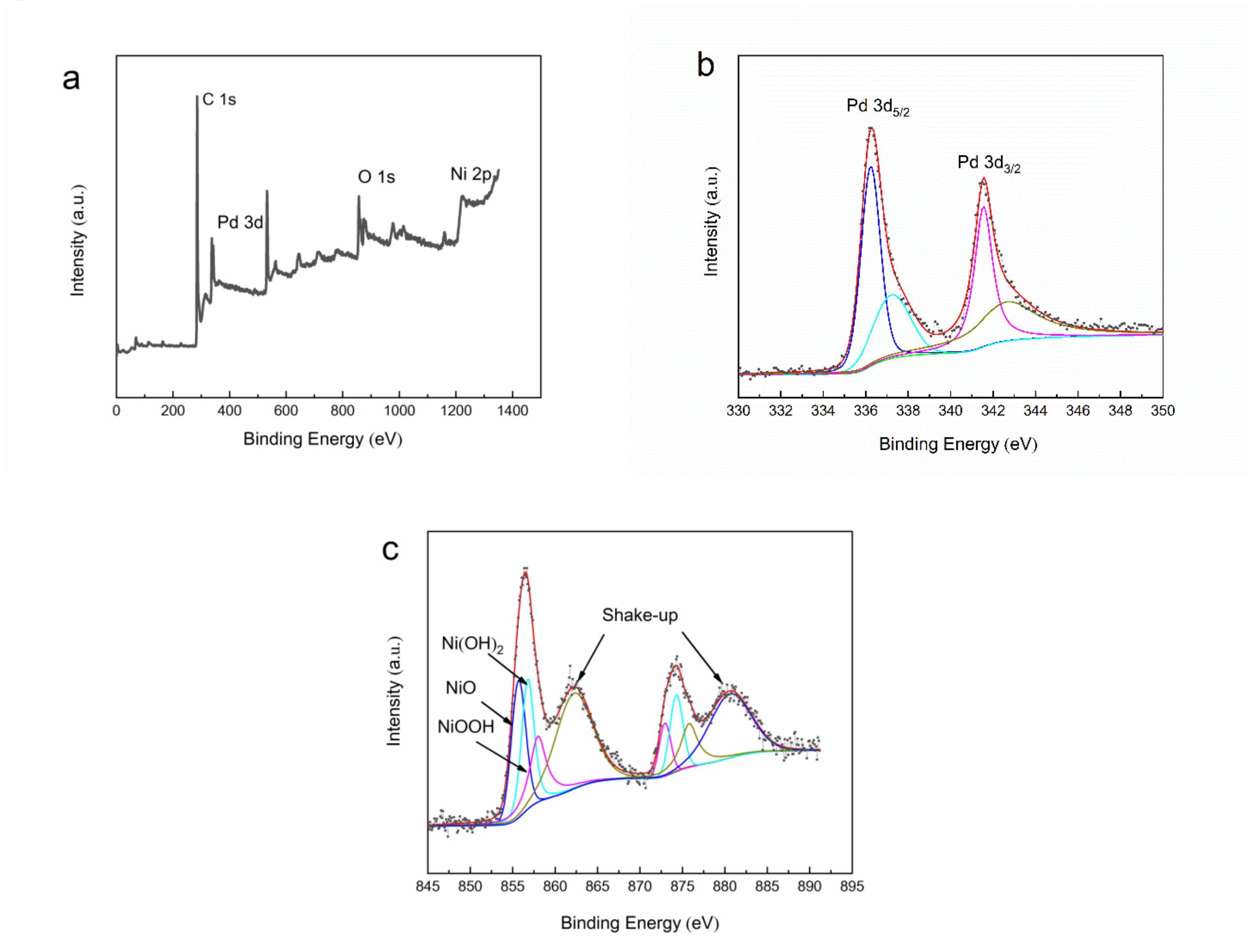

Figure 3. XPS spectra of (a) wide-scan survey of $Pd\text{-}PdH_{0.706}@PdO\text{-}NiO_xH_y/C\text{-}10$, (b) Pd 3d spectrum of $Pd\text{-}PdH_{0.706}@PdO\text{-}NiO_xH_y/C\text{-}10$, (c) Ni 2p spectrum of $Pd\text{-}PdH_{0.706}@PdO\text{-}NiO_xH_y/C\text{-}10$.

An XPS analysis was used to analyse the surface composition and oxidation state of metals in the $Pd\text{-}PdH_{0.706}@PdO\text{-}NiO_xH_y/C\text{-}10$ catalyst. As shown in Fig. 3a, the peak positions at 284.6, 334.8, 533.2 and 856.5 eV are C 1s, Pd 3d, O 1s and Ni 2p, respectively. Fig. 3 (b-c) shows the regional spectra of the Pd 3d and Ni 2p core level regions. The 341.5 and 336.2 eV peaks of Pd in Fig. 3b show that the Pd 3d spectra display a doublet peak, which consists of a high-energy band (Pd $3d_{3/2}$) and a low-energy band (Pd $3d_{5/2}$). These peaks are attributed to the presence of PdO [34-36]. Another doublet of Pd $3d_{5/2}$ and Pd $3d_{3/2}$ peaks at approximately 337.2 and 342.6 eV, respectively, are attributed to a high oxidation state similar to PdO [37]. Therefore, this observation indicates that PdO is the main form of Pd metal on the surface of the catalyst particles. Moreover, the $3d_{5/2}$ peak of Pd is located at 336.2 eV, which is positively shifted by 1.0 eV compared to pure Pd in the literature [38]. This is due to the generation of $PdH_{0.706}$ and the alloying of Ni and Pd, which is consistent with the XPS results. As shown in Fig. 3c, the Ni 2p spectrum of the Pd-$PdH_{0.706}$@PdO-NiO_xH_y/C-10 catalyst also shows a doublet peak, which consists of a high-energy band (Ni $2p_{1/2}$) and a low-energy band (Ni $2p_{3/2}$). The broad Ni $2p_{3/2}$ peak may be assigned to three peaks at 855.6, 856.8 and 858.0eV, which correspond to NiO, $Ni(OH)_2$ and NiOOH, respectively. As a result, Ni metal exists mainly in the form of NiO, $Ni(OH)_2$ and NiOOH on the surface of the catalyst particles [39,40].

3.2 Electrochemical studies

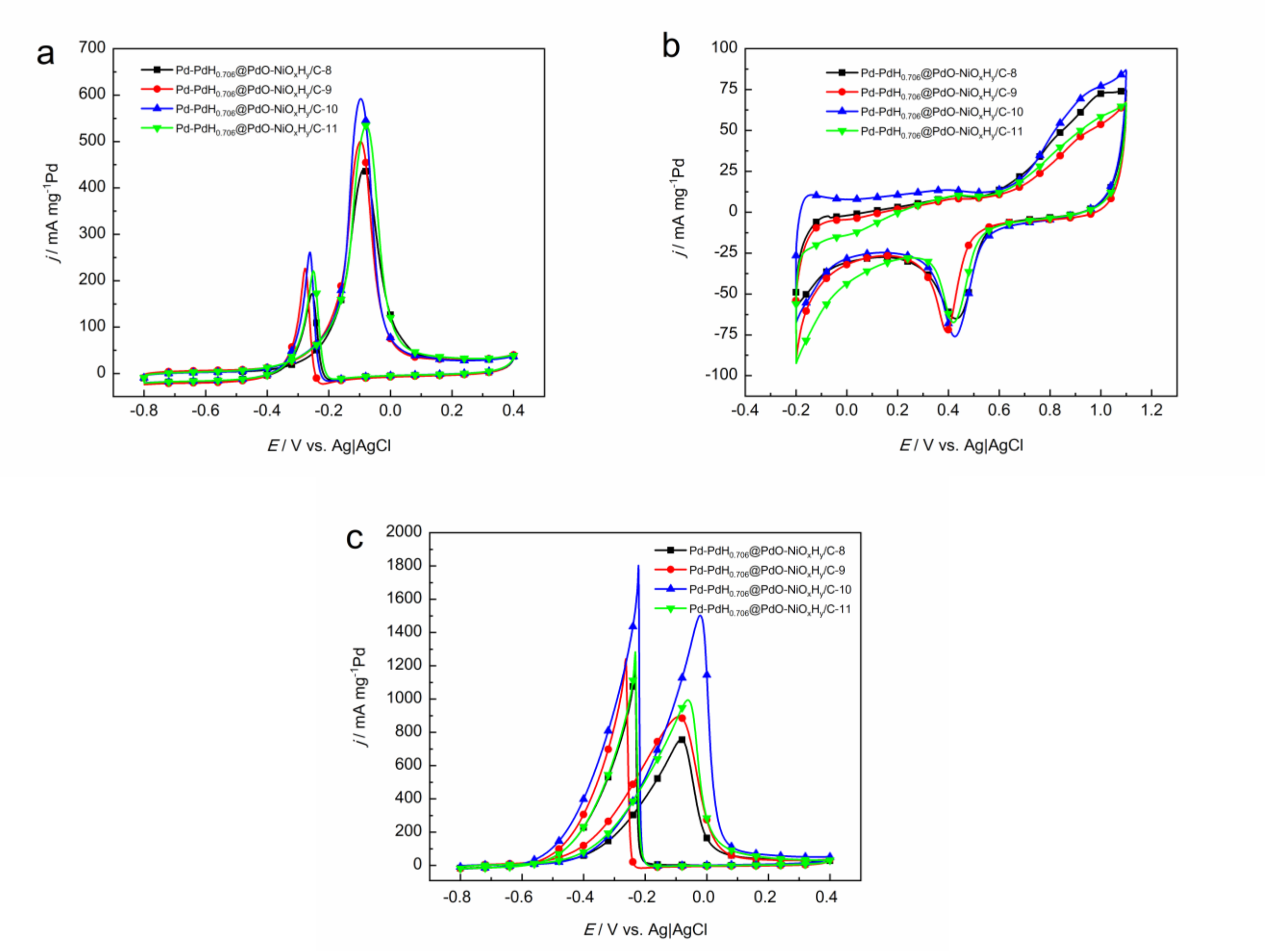

Figure 4. CV curves of the Pd-$PdH_{0.706}$@PdO-NiO_xH_y/C-8, Pd-$PdH_{0.706}$@PdO-NiO_xH_y/C-9, Pd-$PdH_{0.706}$@PdO-NiO_xH_y/C-10 and Pd-$PdH_{0.706}$@PdO-NiO_xH_y/C-11 catalysts in solutions of (a) 0.1 M KOH + 1 M CH_3OH, (b) 0.05 M H_2SO_4, and (c) 0.1 M KOH + 1 M CH_3CH_2OH at 50 mV/s. The present densities are standardized by the actual Pd loadings.

As shown in Fig. 4a, all the catalysts have significant characteristics of methanol oxidation peaks in the anodic scan. The oxidation peak values of methanol on the Pd-$PdH_{0.706}$@PdO-NiO_xH_y/C-8, Pd-$PdH_{0.706}$@PdO-NiO_xH_y/C-9, Pd-$PdH_{0.706}$@PdO-NiO_xH_y/C-10 and Pd-$PdH_{0.706}$@PdO-NiO_xH_y/C-11 catalysts are 439.8, 500.0, 592.1 and 554.5 mA mg^{-1} Pd, respectively. It can be seen that the oxidation peak first increases and then decreases with the increase in the amount of KOH solution. This phenomenon is related to the effect of the distribution and the average size of Pd-based nanoparticles in the Pd-$PdH_{0.706}$@PdO-NiO_xH_y/C catalysts, which is caused by the KOH solution [28]. In addition, the Pd-$PdH_{0.706}$@PdO-NiO_xH_y/C-10 catalyst has the best catalytic performance for methanol oxidation. Compared with other literature on the Pd/C catalyst (367.9 mA mg^{-1} Pd), the Pd-$PdH_{0.706}$@PdO-NiO_xH_y/C catalysts have higher oxidation peak values [41]. This phenomenon indicates that the presence of a sufficient amount of Ni can reduce the occupation of active sites by carbon-containing intermediates such as CO, thereby releasing more active sites and improving the electrocatalytic activity [42]. $Ni(OH)_2$-based electrode materials also have superior electrochemical performance [43]. In addition, Pd-$PdH_{0.706}$ causes a change in the lattice, which increases the carrier mobility [44]. Therefore, the Pd-$PdH_{0.706}$@PdO-NiO_xH_y/C catalysts show more active sites, which provides them with high catalytic activity [45].

By studying the CV curves in 0.05 M H_2SO_4 solution, the electrochemically active surface area (ECSA) of the Pd-$PdH_{0.706}$@PdO-NiO_xH_y/C catalysts[46] can be determined. As shown in Fig. 4b, the cathodic current peak at approximately 0.2-0.6 V can be used to evaluate the ECSA of the catalyst. The ECSA is calculated by measuring the charge collected in the cathodic peak at 0.4 V before a double-layer correction and assuming a value of 0.424 mC/cm^2 for the reduction of the PdO monolayer.

$ECSA = Q/[Pd] * 0.424$ [47]

The ECSAs of the Pd-$PdH_{0.706}$@PdO-NiO_xH_y/C-8, Pd-$PdH_{0.706}$@PdO-NiO_xH_y/C-9, Pd-$PdH_{0.706}$@PdO-NiO_xH_y/C-10 and Pd-$PdH_{0.706}$@PdO-NiO_xH_y/C-11 catalysts are calculated to be 428, 444, 452 and 436 cm^2 mg^{-1} Pd, respectively. The ECSAs first increase and then decrease with increasing amounts of the KOH solution. The Pd-$PdH_{0.706}$@PdO-NiO_xH_y/C-10 catalyst has the largest specific surface area, which is attributed to the good dispersion of the Pd-$PdH_{0.706}$@PdO-NiO_xH_y/C-10 catalyst on the carbon support [48].

Fig. 4c shows the CV curves on the Pd-$PdH_{0.706}$@PdO-NiO_xH_y/C catalysts in 0.1 M KOH + 1 M CH_3CH_2OH. The oxidation peak values of the Pd-$PdH_{0.706}$@PdO-NiO_xH_y/C-8, Pd-$PdH_{0.706}$@PdO-NiO_xH_y/C-9, Pd-$PdH_{0.706}$@PdO-NiO_xH_y/C-10 and Pd-$PdH_{0.706}$@PdO-NiO_xH_y/C-11 catalysts are 756.4, 894.5, 1504.0 and 994.1 mA mg^{-1} Pd, respectively. Due to reactions with intermediate products, a current peak appears at -0.6-0.0 V during the negative scan. It can be seen that the Pd-$PdH_{0.706}$@PdO-NiO_xH_y/C-10 catalyst has the best catalytic performance in ethanol oxidation. This is because $Ni(OH)_2$ and $PdH_{0.706}$ can increase Pd activity, and $Ni(OH)_2$ is also catalytically active towards the oxidation reaction [49].

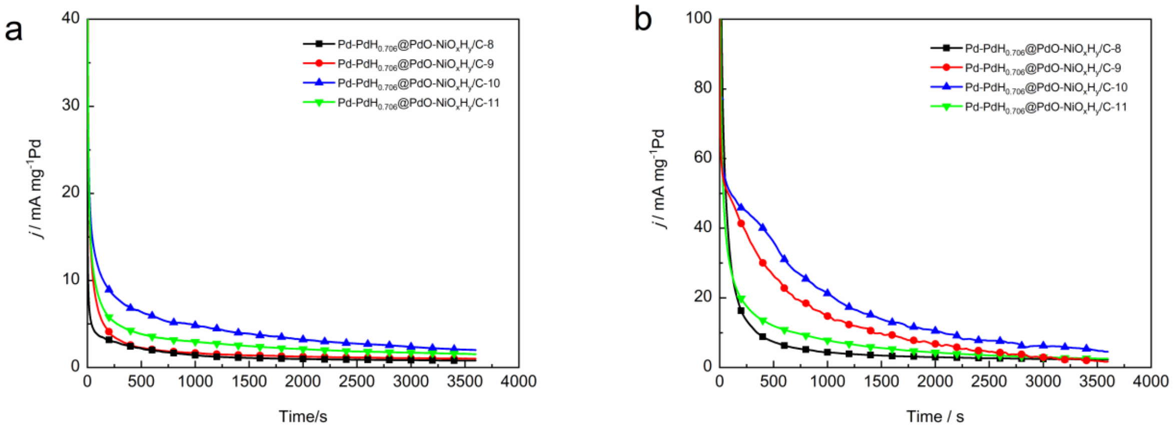

Figure 5. Chronoamperometric curves run at 0.1 V vs. Ag|AgCl on the Pd-PdH$_{0.706}$@PdO-NiO$_x$H$_y$/C-8, Pd-PdH$_{0.706}$@PdO-NiO$_x$H$_y$/C-9, Pd-PdH$_{0.706}$@PdO-NiO$_x$H$_y$/C-10 and Pd-PdH$_{0.706}$@PdO-NiO$_x$H$_y$/C-11 catalysts respectively in the mixed solutions of (a) 0.1 M KOH + 1 M CH$_3$OH and (b) 0.1 M KOH + 1 M CH$_3$CH$_2$OH for 3600 s at 25 °C.

To confirm the stability of the Pd-PdH$_{0.706}$@PdO-NiO$_x$H$_y$/C catalysts, chronoamperometry is an important method. Figure. 5a depicts the chronoamperometric curves of the Pd-PdH$_{0.706}$@PdO-NiO$_x$H$_y$/C catalysts for the electrocatalytic oxidation of methanol in 0.1 M KOH + 1 M CH$_3$OH at 0.1 V. The current densities on the Pd-PdH$_{0.706}$@PdO-NiO$_x$H$_y$/C-8, Pd-PdH$_{0.706}$@PdO-NiO$_x$H$_y$/C-9, Pd-PdH$_{0.706}$@PdO-NiO$_x$H$_y$/C-10 and Pd-PdH$_{0.706}$@PdO-NiO$_x$H$_y$/C-11 catalysts are approximately 0.8, 1.0, 2.2, and 1.53 mA mg^{-1} Pd, respectively. Therefore, the Pd-PdH$_{0.706}$@PdO-NiO$_x$H$_y$/C-10 catalyst also has the best electrocatalytic stability and current density for the methanol electrooxidation after 3600 s. The results show that the Pd-PdH$_{0.706}$@PdO-NiO$_x$H$_y$/C-10 catalyst has the best catalytic stability for the methanol electrooxidation, demonstrating a good resistance to poisoning [50,51].

Table 2. EIS parameters of the catalysts

Catalyst	0.1 M KOH + 1 M CH$_3$OH				0.1 M KOH + 1 M CH$_3$CH$_2$OH			
	R1(ohm)	R2(ohm)	CPE1T(μF)	CPE1P(μF)	R1(ohm)	R2(ohm)	CPE1-T(μF)	CPE1P(μF)
Pd-PdH$_{0.706}$@PdO-NiO$_x$H$_y$/C-8	39.75	15779	0.00011508	0.90527	43.99	15802	0.00021428	0.87448
Pd-PdH$_{0.706}$@PdO-NiO$_x$H$_y$/C-9	39.32	14944	0.00010137	0.90463	39.58	13242	0.0001121	0.90436
Pd-PdH$_{0.706}$@PdO-NiO$_x$H$_y$/C-10	40.38	8525	0.00015714	0.92683	43.58	5113	0.00018984	0.91228
Pd-PdH$_{0.706}$@PdO-NiO$_x$H$_y$/C-11	39.74	13710	0.00010166	0.90483	40.68	15132	0.00014134	0.85615

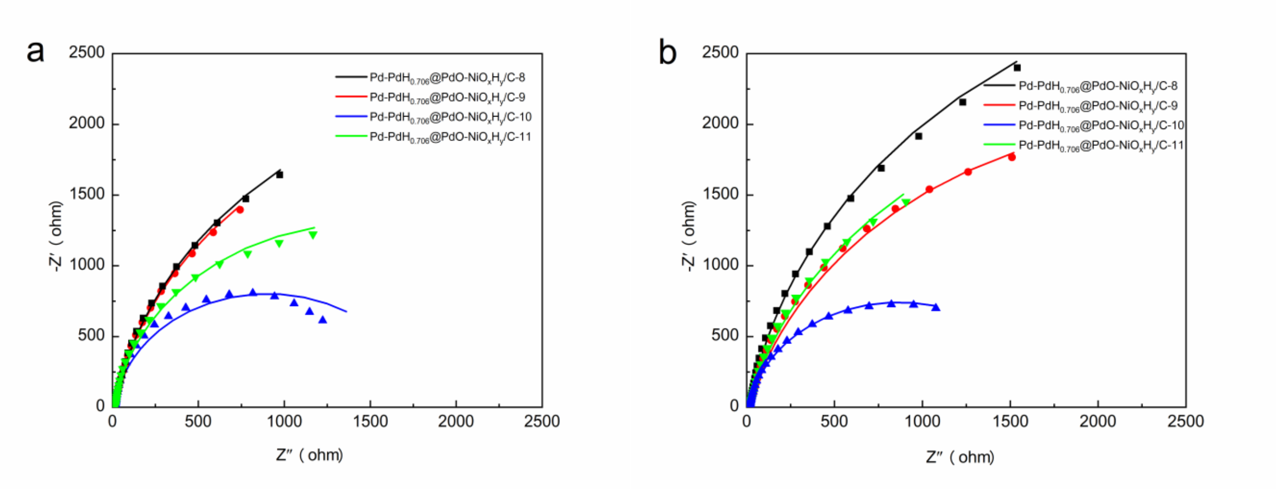

Figure 6. Nyquist plots of electrooxidation on the $Pd-PdH_{0.706}@PdO-NiO_xH_y/C-8$, $Pd-PdH_{0.706}@PdO-NiO_xH_y/C-9$, $Pd-PdH_{0.706}@PdO-NiO_xH_y/C-10$ and $Pd-PdH_{0.706}@PdO-NiO_xH_y/C-11$ catalysts in (a) 0.1 M KOH + 1 M CH_3OH and (b) 0.1 M KOH + 1 M CH_3CH_2OH at -0.1V vs. Ag|AgCl.

In addition, Fig. 5b shows the chronoamperometric curves of these catalysts in 0.1 M KOH + 1 M CH_3CH_2OH. The current densities of the $Pd-PdH_{0.706}@PdO-NiO_xH_y/C-8$, $Pd-PdH_{0.706}@PdO-NiO_xH_y/C-9$, $Pd-PdH_{0.706}@PdO-NiO_xH_y/C-10$ and $Pd-PdH_{0.706}@PdO-NiO_xH_y/C-11$ catalysts are approximately 2.32, 1.67, 4.56, and 2.54 mA mg^{-1} Pd, respectively. The $Pd-PdH_{0.706}@PdO-NiO_xH_y/C-10$ catalyst still has the highest current density. However, among the other three catalysts, the chronoamperometric curve of the $Pd-PdH_{0.706}@PdO-NiO_xH_y/C-9$ catalyst has a relatively high initial value and the minimum value after 3600 s. This is caused by an unstable step voltage applied to the working electrode [52]. Based on the above structural analyses, we may attribute the outstanding current density of $Pd-PdH_{0.706}@PdO-NiO_xH_y/C-10$ to the high electrochemical activity of $Pd-PdH_{0.706}$ and $Ni(OH)_2$, thereby enhancing the performance [38].

As shown in Fig. 6, EIS is used to analyse the electrocatalytic reaction of each electrode in different solutions. R1 and R2 embody electrochemical reactions, and CPE1 is the double-layer capacitance for the electrochemical reactions. The value of R2 is related to the radius of the arc in Table 2. Due to a small arc radius, the electron transfer resistance is small, and thus, the catalytic performance is better. The impedance data are provided in Table 2, which simply indicates that the $Pd-PdH_{0.706}@PdO-NiO_xH_y/C-10$ catalyst has the smallest charge transfer resistance in Fig. 6a and Fig. 6b and shows the best performance. The observed high dispersion of $Pd-PdH_{0.706}@PdO-NiO_xH_y/C-10$ will likely decrease the build-up of methanol and ethanol reaction intermediates and increase the further adsorption of methanol and ethanol on the electrode surface [24].

4. CONCLUSIONS

An easy and reproducible one-pot synthesis of Pd−Ni core-shell nanoalloys is presented. The $Pd-PdH_{0.706}@PdO-NiO_xH_y/C$ nanocatalyst is synthesized using TBA. As shown in the characterization of the Pd-PdH$_{0.706}$@PdO-NiO$_x$H$_y$/C catalysts, Pd-Ni nanoparticles are successfully deposited on the surface of the carbon support, and Pd-PdH$_{0.706}$ is synthesized on the activated carbon. The average diameter of the nanoparticles in the Pd-PdH$_{0.706}$@PdO-NiO$_x$H$_y$/C catalysts is approximately 10 nm. In addition, the geometric structure of the particles is mostly spherical and shows a core-shell structure with PdO-NiO as the shell and Pd-PdH$_{0.706}$ as the core. Moreover, Ni(OH)$_2$ and PdH$_{0.706}$ can increase Pd activity, and Ni(OH)$_2$ is catalytically active towards the methanol oxidation reaction. The Pd-PdH$_{0.706}$@PdO-NiO$_x$H$_y$/C catalyst with good activity can be prepared with an appropriate amount of KOH solution. The Pd-PdH$_{0.706}$@PdO-NiO$_x$H$_y$/C-10 catalyst has the smallest particle size and has the best catalytic performance in ethanol oxidation and methanol oxidation. In chronoamperometry and EIS tests, the Pd-PdH$_{0.706}$@PdO-NiO$_x$H$_y$/C-10 catalyst demonstrates its durability and still shows a good current density and charge transfer rate. The above results indicate that the Pd-PdH$_{0.706}$@PdO-NiO$_x$H$_y$/C-10 catalyst will be useful as an efficient and economical anode catalyst in the development of DMFCs.

ACKNOWLEDGEMENT
We would like to thank the Major Science and Technology Project of Shanxi (20181102019) for funding.

References

1. O.Karatepe, Y. Yıldız, H. Pamuk, S. Eris, Z. Dasdelen and F. Sen, *RSC Adv*, 6 (2016) 50851.
2. S. Eris, Z. Daşdelen and F. Sen, *J Colloid Interf Sci*, 513 (2018) 767.
3. C. Won Choon, J. Min Ku, K. Yo Jin, W. Seong Ihl and H. Won Hi, *Catal. Today*, 93-95 (2004) 517.
4. M.G. Hosseini, M.M. Momeni and M. Faraji, *Electroanalysis*, 22 (2010) 2620.
5. U.B. Demirci, *J. Power Sources*, 173 (2007) 11.
6. S. Basri, S.K. Kamarudin, W.R.W. Daud and Z. Yaakub, *Int J Hydrogen Energ*, 35 (2010) 7957.
7. Y. Li, W. Gao, L. Ci, C. Wang and P.M. Ajayan, *Carbon*, 48 (2010) 1124.
8. S.M. Choi, M.H. Seo, H.J. Kim and W.B. Kim, *Carbon*, 49 (2011) 904.
9. K. Bergamaski, E.R. Gonzalez and F.C. Nart, *Electrochim. Acta*, 53 (2008) 4396.
10. T. Kawaguchi, W. Sugimoto, Y. Murakami and Y. Takasu, *J. Catal.*, 229 (2005) 176.
11. I. Cabria, J.M. López and A.J. Alonso, *Phys Rev B*, 81 (2010) 5403.
12. I. Saldan, Y. Semenyuk, I. Marchuk and O. Reshetnyak, *J Mater Sci*, 50 (2015) 2337.
13. G. Shaojun, D. Shaojun and W. Erkang, *ACS Nano*, 4 (2010) 547.
14. H. Huang and X. Wang, *J. Mater. Chem.*, 22 (2012) 22533.
15. Z. Xiang, D. Yan, J. Hong, L. Yefei and C. Rizhi, *Catal. Lett.*, 149 (2019) 813.
16. S. Yan, L. Gao, S. Zhang, L. Gao, W. Zhang and Y. Li, *Int J Hydrogen Energ*, 38 (2013) 12838.
17. Y. Koskun, A. Savk, B. Sen and F. Sen, *Anal. Chim. Acta*, 1010 (2018) 37.
18. K. Lee, S.W. Kang, S.-U. Lee, K.-H. Park, Y.W. Lee and S.W. Han, *ACS Appl Mater Inter*, 4 (2012) 4208.
19. S. Wang, D. Tian, X. Wang, J. Qin, Y. Tang, J. Zhu, Y. Cong, H. Liu, Y. Lv, C. Qiu, Z. Gao and Y. Song, *Electrochem. Commun.*, 102 (2019) 67.
20. Y. Lu, J. Wang, Y. Peng, A. Fisher and X. Wang, *Adv Energy Mater*, 7 (2017) 1700919.
21. M.A. Bhosale, T. Sasaki and B.M. Bhanage, *Powder Technol.*, 291 (2016) 154.
22. K. Ding, H. Yang, Y. Cao, C. Zheng, S.B. Rapole and Z. Guo, *Mater. Chem. Phys.*, 142 (2013) 403.
23. R. Li, Z. Wei, T. Huang and A. Yu, *Electrochim. Acta*, 56 (2011) 6860.

24. T. Ramulifho, K.I. Ozoemena, R.M. Modibedi, C.J. Jafta and M.K. Mathe, *Electrochim. Acta*, 59 (2012) 310.
25. H.S. Liu, C.J. Song, L. Zhang, J.J. Zhang, H.J. Wang and D.P. Wilkinson, *J. Power Sources*, 155 (2006) 95.
26. T. Jianhua, S. Jianfeng, L. Na and Y. Mingxin, *Ceram. Int.*, 41 (2015) 6203.
27. E. Guan, A.C. Foucher, N. Marcella, T. Shirman, M. Luneau, A.R. Head, D.M.A. Verbart, J. Aizenberg, C.M. Friend, D. Stacchiola, E.A. Stach and A.I. Frenkel, *ChemCatChem*, 10 (2019) 1002.
28. Y. Shaofeng, H. Qiong, Y. Yingjia, M. Xuli, G. Lizhen, Y. Shaohui, W. Yucheng and L. Liquan, *Int J Electrochem Sc*, 14 (2019) 7871.
29. F.P. Hu and P.K. Shen, *J. Power Sources*, 173 (2007) 877.
30. X. Zhu, H. Dai, J. Hu, L. Ding and L. Jiang, *J. Power Sources*, 203 (2012) 243.
31. Z. Zhao, X. Huang, M. Li, G. Wang, C. Lee, E. Zhu, X. Duan and Y. Huang, *J. Am. Chem. Soc.*, 137 (2015) 15672.
32. T. Maiyalagan and S. Keith, *J. Power Sources*, 195 (2010) 5246.
33. L. Ma, H. He, A. Hsu and R. Chen, *J. Power Sources*, 241 (2013) 696.
34. M.H. Seo, S.M. Choi, J.K. Seo, S.H. Noh, W.B. Kim and B. Han, *Appl Catal B-Environ*, 129 (2013) 163.
35. A. Mondal and N.R. Jana, *ACS Catalysis*, 4 (2014) 593.
36. Y. Yingjia, Y. Shaofeng, G. Lizhen, W. Xiaomin and Y. Shaohui, *Int J Electrochem Sc*, 14 (2019) 1270.
37. K. Ding, J. Han, X. Gao, L. Wang, L. Zhou, R. Qu and X. He, *Int J Hydrogen Energ*, 45 (2020) 1930.
38. Y. Wang, F.-F. Shi, Y.-Y. Yang and W.-B. Cai, *J. Power Sources*, 243 (2013) 369.
39. S.Y. Shen, T.S. Zhao, J.B. Xu and Y.S. Li, *J. Power Sources*, 195 (2010) 1001.
40. T. Liu, C. Jiang, B. Cheng, W. You and J. Yu, *J. Power Sources*, 359 (2017) 371.
41. R. Awasthi and R.N. Singh, *Carbon*, 51 (2013) 282.
42. H. Huang, H. Wang, W. Hu, W. Lv and W. Ye, *Electrochem. Commun.*, 82 (2017) 107.
43. P. Lu, F. Liu, D. Xue, H. Yang and Y. Liu, *Electrochim. Acta*, 78 (2012) 1.
44. S. Fonseca, G. Maia and L.M.C. Pinto, *Electrochem. Commun.*, 93 (2018) 100.
45. Y. Wang, Y. Zhao, J. Yin, M. Liu, Q. Dong and Y. Su, *Int J Hydrogen Energ*, 39 (2014) 1325.
46. S. Yan and S. Zhang, *Int J Hydrogen Energ*, 37 (2012) 9636.
47. S. Dutta, C. Ray, A. Roy, R. Sahoo and T. Pal, *Chemistry*, 22 (2016) 10017.
48. L. Jiang, A. Hsu, D. Chu and R. Chen, *Int J Hydrogen Energ*, 35 (2010) 365.
49. N.A.M. Barakat, M. Motlak, A.A. Elzatahry, K.A. Khalil and E.A.M. Abdelghani, *Int J Hydrogen Energ*, 39 (2014) 305.
50. L.Y. Chen, N. Chen, Y. Hou, Z.C. Wang, S.H. Lv, T. Fujita, J.H. Jiang, A. Hirata and M.W. Chen, *ACS Catalysis*, 3 (2013) 1220.
51. S. Yan and S. Zhang, *Int J Hydrogen Energ*, 36 (2011) 13392.
52. M.S. Ahmed and S. Jeon, *ACS Catalysis*, 4 (2014) 1830.